Numerical and Semi-Empirical Prediction of Zero-Lift Drag Coefficient of a Small Caliber Spinning Projectile: A Comparative Investigation

Q. T. Nguyen[1,*]

[1]Faculty of Special Equipment, Le Quy Don Technical University, Hanoi, 100000, Vietnam

ABSTRACT: This paper focuses on a comparative performance evaluation of the numerical and semi-empirical methods in predicting the zero-lift drag of a generic small calibre spinning projectile. The numerical simulations of the flow around the projectile, namely, the 5.69 mm BRL-1 projectile were conducted using Reynolds-Averaged Navier-Stokes equations with Shear Stress Transport k-ω turbulence model. The simulation results were validated against existing experimental data. The McCoy's method was applied for semi-empirical prediction of zero-lift drag of the projectile. The pressure drag, skin friction drag and base drag components of the total aerodynamic drag of the projectile at various Mach numbers were also investigated in this study. The aerodynamic drags obtained using numerical and semi-empirical methods were compared to show strengths and shortcomings of each approach. The average difference between numerical and experimental zero-lift drag coefficients is 1.74%, while the corresponding value for semi-empirical and experimental zero-lift drag coefficients is 5.31%.

KEYWORDS: Spinning projectile, Drag, CFD, Aerodynamics, Numerical simulation, Semi-empirical.

[Received Jan. 17, 2025; Revised Sep. 02, 2025; Accepted Oct. 12, 2025] Print ISSN: 0189-9546 | Online ISSN: 2437-2110

I. INTRODUCTION

Aerodynamic drag is an important parameter for calculating the trajectory of a projectile. There are three methods available for the determination of aerodynamic drag acting on a projectile, namely, experimental, semi-empirical, and Computational Fluid Dynamics (CFD) methods (McCoy, 2009). Although experimental methods provide the most accurate results, they are the most expensive and time-consuming. Hence, experimental methods are usually used in the final stages of projectile design process. The advantage of the semi-empirical method is that they can give the results very quickly, though these results are least accurate compared to other methods (De Briey, 2021). However, semi-empirical methods are very useful in the initial stages of the design process allowing the researchers promptly access the different design variations. In recent years, with the rapid advance in computer technology and numerical methods, the CFD method has become a very effective and widely used numerical tool to simulate and analyse the fluid flow phenomena. Currently, researchers and engineers around the world are applying these three approaches to solve different aerodynamic problems. Pokela *et al.* (2021) experimentally studied aerodynamic characteristics of axisymmetric projectile configurations at supersonic speeds. Mahdi *et al.* (2008) used semi-empirical approach to investigate the effect of body shape on the aerodynamics of projectiles at supersonic speeds. Moore *et al.* (2002) applied semi-empirical method for prediction of base drag. The semi-empirical method based DATCOM software was employed by Vasile *et al.* (2020) for the aerodynamic optimisation of long-range projectiles. Seretkaya *et al.* (2022) predicted total drag coefficient of 155 mm projectile using both numerical simulation and semi-empirical approaches. Nguyen *et al.* (2024) implemented numerical method for investigating the drag coefficient of a saboted projectile under different conditions. The aerodynamic characteristics of a 120 mm spinning projectile was predicted and analysed by Ko *et al.* (2020) using CFD method. However, it is crucial to understand the advantages and limitations of each approach in order to optimise the design process. Therefore, the primary objective of this study is to evaluate the capability of semi-empirical and numerical methods in prediction of zero-yaw drag of a small calibre spinning projectile.

II. MATERIALS AND METHODS

A. Projectile geometry model

The 5.69 mm BRL-1 projectile is a low-drag small calibre projectile with the total length of 31.18 mm, consisting of a secant ogive nose, a bearing cylinder and a boattail. Its nose length is 17.07 mm with the ogive generating radius of 105.55 mm. The projectile bearing cylinder diameter is 5.69 mm, boattail length of 5.69 mm with a 7-degree boattail angle. It has been used for aerodynamic research in Ballistic Research Laboratories for many years. Its aerodynamic drag investigation has been carried out experimentally (Braun, 1973) and semi-empirically (McCoy, 1981). The projectile configuration reproduced from available literature (McCoy, 1981) is presented in Figure 1. The BRL-1 projectile 3D model created in Inventor CAD software (Figure 2) was imported into

*Corresponding author: *tuannguyenmta28@gmail.com*

doi: http://doi.org/10.63746/njtd.v22i5.3294

the Ansys Fluent software for the following simulation process.

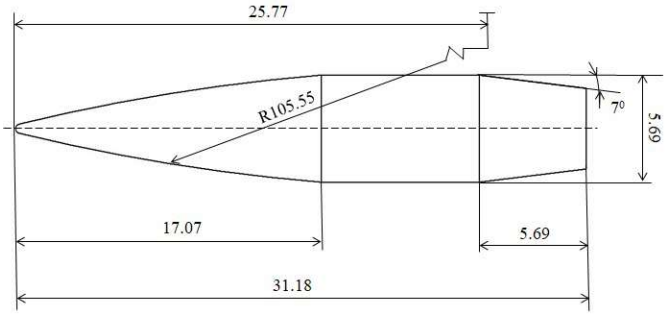

Figure 1 Configuration of BRL-1 projectile (in mm)

Figure 2 3D model of BRL-1 projectile (McCoy, 1981)

B. Semi-empirical method

The semi-empirical method utilised in this paper is the method developed by McCoy (1981) and frequently used for aerodynamic characterisation of different kinds of projectiles. According to this method, the total zero-lift drag coefficient of a spinning projectile can be broken down into several components as follows:

$$C_{D0} = C_{DN} + C_{DBT} + C_{DB} + C_{DRB} + C_{DSF} \quad (1)$$

Where C_{D0} is total zero-lift drag coefficient of the projectile; C_{DN} is pressure drag coefficient due to projectile nose; C_{DBT} is pressure drag coefficient due to projectile boattail; C_{DB} is pressure drag coefficient due to projectile blunt base; C_{DRB} is pressure drag coefficient due to rotating band; C_{DSF} is skin friction drag coefficient.

In this case, since there is no rotating band on the body of the small caliber projectile, the pressure drag coefficient due to rotating band is zero. That means the total drag coefficient of BRL-1 projectile reduced to only four components as follows:

$$C_{D0} = C_{DN} + C_{DBT} + C_{DB} + C_{DSF}, \quad (2)$$

The calculation procedure for each aerodynamic drag component was described in detail by McCoy (1981). This semi-empirical method continues to be widely used as a baseline in modern projectile aerodynamics, particularly for comparisons with CFD or experimental data. Wanchai (2014) demonstrated the successful application of McCoy's method for estimating drag components during the aerodynamic shape optimisation of a supersonic generic round-shaped body. In another study, the aerodynamic drag of a 155 mm projectile under axisymmetric flow was investigated using both CFD and McCoy's semi-empirical approach. The semi-empirical predictions achieved reasonable accuracy, with average deviations of about 5–6% from reference data, whereas the CFD approach reached higher accuracy (≈2%). These results confirm the continued relevance of McCoy's method as a rapid baseline tool for aerodynamic estimations (Ferfouri *et a*l., 2023). In that research, the semi-empirical predictions for the BRL-1 projectile were reproduced from the results originally reported by McCoy (1981) to enable comparative performance analysis.

C. Numerical method

In this study, Ansys Fluent was employed to determine the aerodynamic drag of BRL-1 projectile.

1) Computational domain

The computational domain was initialised in a cuboid form with 40xL of length, 10xL of width, and 10xL of height. Where L is the total length of BRL-1 projectile. The computational domain was created with a size large enough to accurately capture the aerodynamic phenomena occurring at the vicinity of the projectile surface and in the region directly behind the base of the projectile. The projectile model was located on the symmetrical longitudinal axis of the simulation domain and is 15xL away from the Inlet boundary and 24xL Outlet boundary respectively as shown in Figure 3.

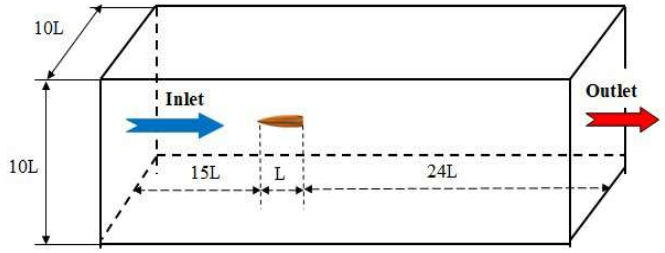

Figure 3 The computational domain

2) Turbulence model

In the present research, Shear Stress Transport (SST) *k-ω* turbulence model was utilized for numerical simulations. This two-equation eddy-viscosity turbulence model, originally developed by Menter in 1994 (Menter, 1994), was adopted to capture the flow characteristics accurately. It has been used by many engineers and researchers for a wide variety of aerodynamic applications. This turbulence model blends standard *k-ε* and standard *k-ω* models to combine their advantages for enhancing the simulation accuracy. The two transport equations of SST *k-ω* turbulence model are defined as follows:

$$\frac{\partial}{\partial t}(\rho k) + \frac{\partial}{\partial x_i}(\rho k u_i) = \frac{\partial}{\partial x_j}\left(\Gamma_k \frac{\partial k}{\partial x_j}\right) + G_k - Y_k + S_k \quad (3)$$

$$\frac{\partial}{\partial t}(\rho \omega) + \frac{\partial}{\partial x_i}(\rho \omega u_i) = \frac{\partial}{\partial x_j}\left(\Gamma_\omega \frac{\partial \omega}{\partial x_j}\right) + G_\omega - Y_\omega + D_\omega + S_\omega \quad (4)$$

where G_k is the turbulence kinetic energy due to the mean velocity gradients; G_ω is the generation of ω; Γ_k and Γ_ω are respectively the effective diffusivity of k and ω; Y_k and Y_ω are respectively the dissipations of k and ω due to the turbulence; S_k and S_ω are the user-defined source terms; D_ω is the the cross-diffusion term; D_ω is the the cross-diffusion term.

The turbulent viscosity μt is computed as follows:

$$\mu_t = \frac{\rho k \alpha_1}{\max\left[\alpha_1 \omega,\ SF_2\right]}, \tag{5}$$

Where α_1 is a constant of the turbulence model, S is the strain rate magnitude, F_2 is a blending function. In the SST k-ω model, the turbulent Prandtl numbers σ_k and σ_ω are determined as:

$$\sigma_k = \frac{1}{\frac{F_1}{\sigma_{k,1}} + \frac{1-F_1}{\sigma_{k,2}}},\ \sigma_\omega = \frac{1}{\frac{F_1}{\sigma_{\omega,1}} + \frac{1-F_1}{\sigma_{\omega,2}}} \tag{6}$$

where F_1 is a blending function; $\sigma_{k,1}$, $\sigma_{k,2}$, $\sigma_{\omega,1}$, and $\sigma_{\omega,2}$ are constants. The parameters G_k and G_ω are calculated as:

$$G_k = min\left(G_k, 10\rho\beta^* k\omega\right),\ G_\omega = \frac{\alpha}{\upsilon_t} G_k, \tag{7}$$

The cross-diffusion term D_ω is defined as follows:

$$D_\omega = 2\left(1-F_1\right)\rho\sigma_{\omega,2}\frac{1}{\omega}\frac{\partial k}{\partial x_j}\frac{\partial \omega}{\partial x_j} \tag{8}$$

The constants of the model are as follows: $\sigma_{k,1} = 1.176$, $\sigma_{\omega,1} = 2.0$, $\sigma_{k,2} = 1.0$, $\sigma_{\omega,2} = 1.168$, $\beta_{i,1} = 0.075$, $\beta_{i,2} = 0.0828$, $\beta^* = 0.09$, $k = 0.41$.

3) Solver setup and boundary conditions

Ansys Fluent software package (Matsson, 2023) with SST *k-ω* turbulence model was applied in this research to simulate the flow around BRL-1 projectile. The Coupled algorithm was adopted for the study. The air is defined as ideal gas. The three component Sutherland model was implemented to model air viscosity. The boundary conditions that need to be specified are inlet, outlet, and wall. Pressure far field was set for the Inlet flow. Outlet boundary condition was set as the Pressure outlet. The wall was modelled as non-slip wall boundary. The conditions for atmosphere parameters were defined as follows: $p_0 = 101325\ Pa$ and $T_0 = 288{,}16\ K$. The simulation results were deemed converged when the flow residuals had decreased at least 3 orders of magnitude and the zero-yaw drag coefficient changed less than 1% for the last 100 iterations (Salunke *et al*., 2023).

4) Mesh independence study

Before conducting numerical simulations, it is necessary to perform a mesh independence study to ensure the simulation results do not depend on meshing procedure. Six mesh structures with different resolutions were initiated by amending the element sizes on the projectile surface and in the surrounding computation region. Numerical simulations were undertaken at the Mach number of 2.0 with the same boundary conditions and solver setup as above presented. The influence of mesh size on the simulated zero-lift drag coefficient was shown in Figure 4. Obviously, from the mesh size of 3.658 million of cells (Mesh 4) further increase in mesh size will not affect the simulation result. Therefore, Mesh 4 was adopted in this study to simulate the flow around BRL-1 projectile to ensure reasonable accuracy with proper computation time.

In Mesh 4, the mesh was the finest on the projectile surface with the maximum cell size of 0.15 mm and gets coarser from the region near the projectile surface to the boundaries with the maximum cell size of 5 mm. To make sure the dimensionless distance y+ is less than 1, a 15-layer inflation with the first cell height of $2.5\text{x}10^{-4}$ mm from the projectile surface and with a growth rate of 1.15 was employed to better capture the aerodynamics processes occurring at the vicinity of the projectile surface and in the base region. The mesh used in this study was presented in Figure 5.

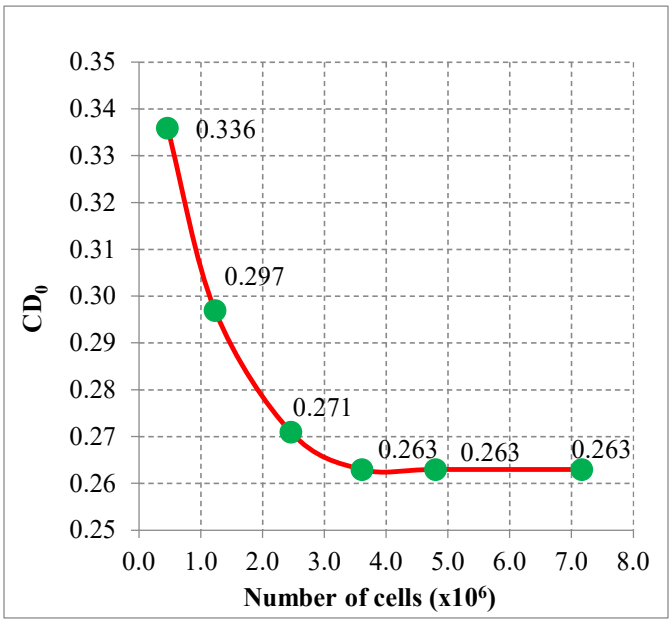

Figure 4 Total zero-lift drag coefficient versus mesh size

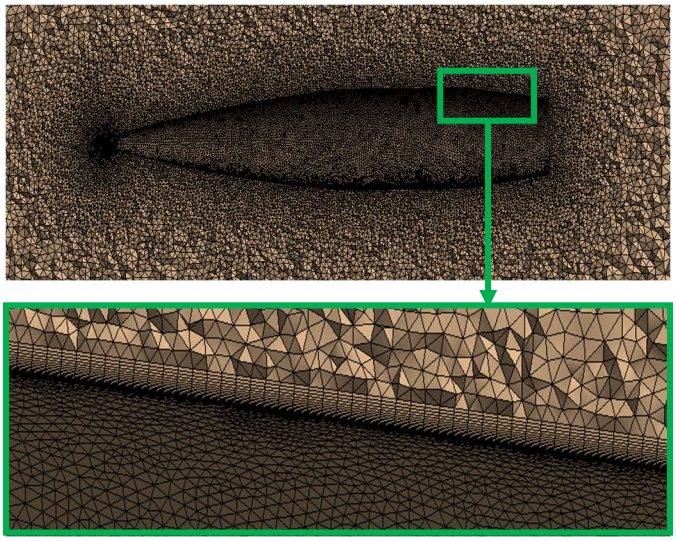

Figure 5 Computational domain mesh (top) and a zoom-in view of the mesh in the vicinity of the projectile surface with inflation layers (bottom)

III. RESULTS AND DISCUSSION

To compare the performance of numerical and McCoy semi-empirical methods at supersonic speeds, BRL-1 projectile total drag coefficient and its components were numerically predicted at Mach numbers ranging from 1.2 to 2.8 with an increment of 0.2. The angle of attack remains zero

for all simulations. The semi-empirically calculated total drag coefficient and its components were based on McCoy computations (McCoy, 1981). The prediction results and their comparative analysis will be discussed in this section.

A. Comparative performance of numerical and semi-empirical prediction methods

1) Total zero-lift drag coefficient

The total zero-lift drag coefficient is one of the most important aerodynamic characteristics. It is needed in solving the fundamental problem of exterior ballistics of projectiles. Therefore, determination of zero-lift drag coefficient is a central task of projectile aerodynamics. In this study, the obtained total drag coefficients at different Mach numbers are compared against existing experimental data to access the effectiveness of each approach. The semi-empirically calculated total drag coefficients at different Mach numbers and their comparison to experimental data are presented, among other, in Table 1. Obviously, the semi-empirically calculated total drag coefficients are slightly lower than the corresponding experimental coefficients for all Mach number investigated. That means the McCoy's approach tends to underpredict the total drag. However, the deviations are acceptable for engineering applications. Specifically, the maximum deviation between semi-empirically calculated and experimental total drag coefficients is 6.94% and the minimum deviation is 3.88%. The average deviation of calculated drag coefficients from the experimental values is 5.31% for the entire Mach number interval investigated, which indicates good agreement of calculated values with the experimental data.

Table 1 Comparison of semi-empirically predicted drag coefficients with experimental data

M	C_{D0}		Deviation (%)	Average deviation (%)
	Experimental method	Semi-empirical method		
1.2	0.332	0.316	4.82	5.31
1.4	0.309	0.297	3.88	
1.6	0.289	0.276	4.50	
1.8	0.272	0.258	5.15	
2.0	0.259	0.242	6.56	
2.2	0.245	0.228	6.94	

The numerically predicted total drag coefficients and their comparison to experimental data under different conditions are presented in Table 2. An excellent agreement between predicted results and experimental data can be observed. In addition, the numerical simulation method tends to overpredicted total drag coefficients at Mach number lower than 2.2 and slightly underpredicted at Mach number greater than or equal 2.2. Quantitatively, the biggest discrepancy between the predicted total drag coefficients and the corresponding experimental values is 2.77% and the lowest discrepancy is 0.85%. Overall, the average discrepancy between the predicted drag coefficients and the experimental data for the entire set of Mach numbers investigated is 1.74%. Generally speaking, both semi-empirical and numerical methods are capable of predicting total zero-lift drag coefficient but with varying accuracy. The numerical method is more accurate showing less deviation from the experimental data compared to the semi-empirical method.

Table 2 Comparison of numerically predicted drag coefficients with experimental data

M	C_{D0}		Deviation (%)	Average deviation (%)
	Experimental method	Numerical method		
1.2	0.332	0.339	2.11	1.74
1.4	0.309	0.316	2.26	
1.6	0.289	0.297	2.77	
1.8	0.272	0.279	2.57	
2.0	0.259	0.263	1.54	
2.2	0.245	0.242	1.22	
2.4	0.234	0.232	0.85	
2.6	0.223	0.221	0.90	
2.8	0.214	0.211	1.40	

For the direct visualization of how the predicted drag coefficients are close to the corresponding experimental values, the results of semi-empirical and numerical predictions are presented as functions of Mach number in Figure 6 along with the experimental data. Evidently, the curves representing the numerically predicted and experimental drag coefficients are very close to each other for the entire Mach number interval investigated. Meanwhile, the curve of semi-empirically predicted values is located more far away from the curve of the experimental data compared to the curve of the numerical method. That means the differences between the semi-empirical and experimental results are significant. Moreover, it can be seen that three curves on the graph follow the same trend showing constant decrease in value with the increase in Mach number.

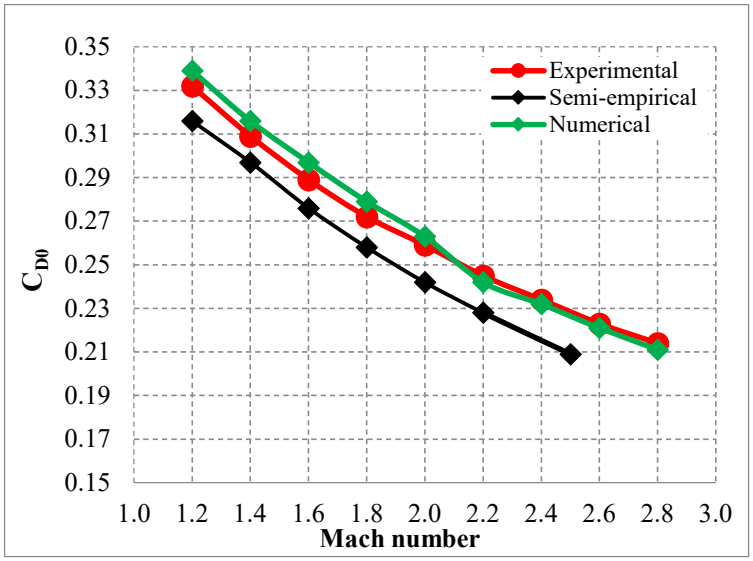

Figure 6 Total zero-lift drag coefficient versus Mach number with different prediction methods

2) Zero-lift drag coefficient components

It is well known from aerodynamics that the total drag force acting on a flying object is the sum of pressure drag and friction (viscous) drag. Pressure drag is resulted from the normal stress exerted by the air pressure force on the object surface, while friction drag is due to the shear stresses brought about by viscosity at the surface of the flying object. Hence, it is interesting and necessary to analyse the variation of each component under different conditions. In the current work, the total drag coefficient components predicted with semi-empirical and numerical simulation methods as functions of Mach number are presented in Figure 7 and Figure 8 respectively. Clearly, the corresponding components obtained with two methods follow the same trends of variation. Among these components, the pressure drag coefficient due to projectile nose C_{DN} is the most dominant accounting for up to about 40% of the total drag coefficient. The second most dominant component is the pressure drag coefficient due to blunt base C_{DBT} which can account for up to nearly 30% in the interval of Mach number investigated. These conclusions are valid for both methods.

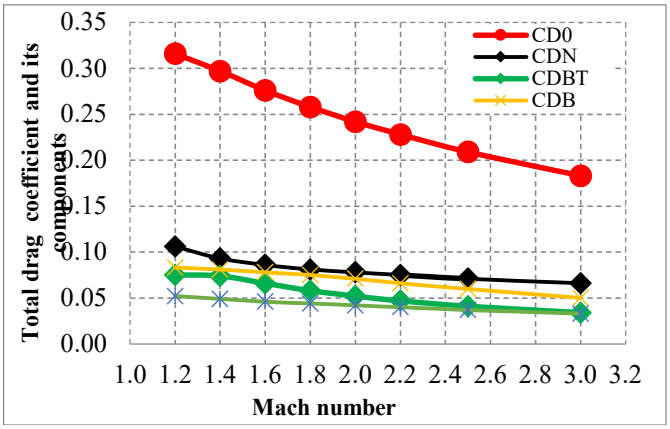

Figure 7 Total zero-lift drag coefficient and its components versus Mach number predicted using semi-empirical method

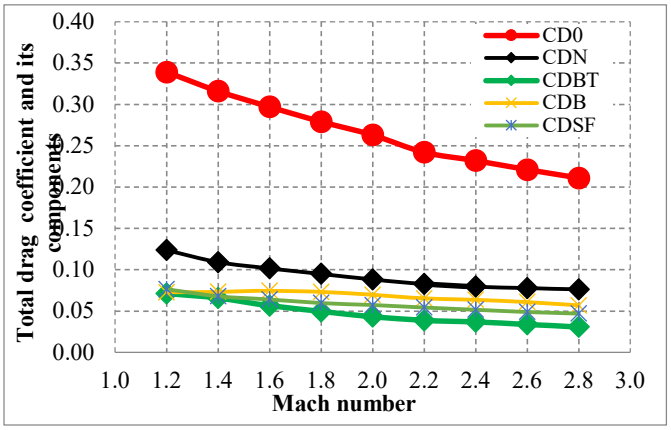

Figure 8 Total zero-lift drag coefficient and its components versus Mach number predicted using numerical method

B. Visualisation of the supersonic flow around the projectile

One of the most noticeable advantages of the numerical simulation method is the ability to visualize the flow field around the projectile which semi-empirical does not possess. Direct visualization of the flow field helps researchers deeper understand the phenomena occurring when the air flow interacts with the flying object. Based on proper assessment of the flow field, one can make appropriate decisions to affect the flow for achieving desired purpose. In this paper, the flow field around BRL-1 projectile represented by the distribution of different flow parameters at Mach number of 2.0 is shown in Figure 9.

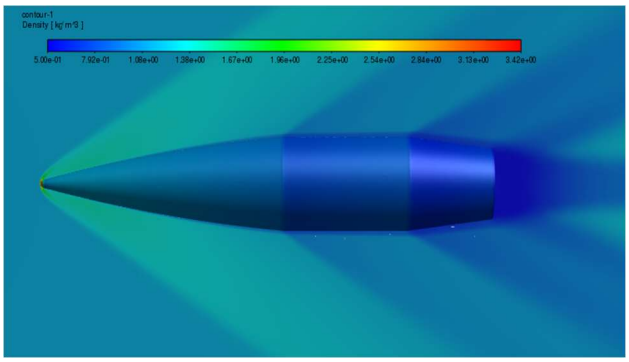

a) Density distribution around the projectile

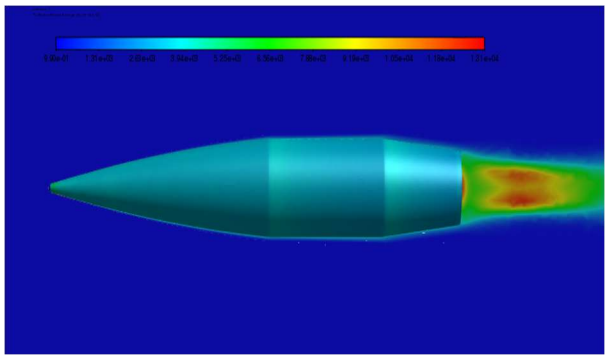

b) Turbulence intensity distribution around the projectile

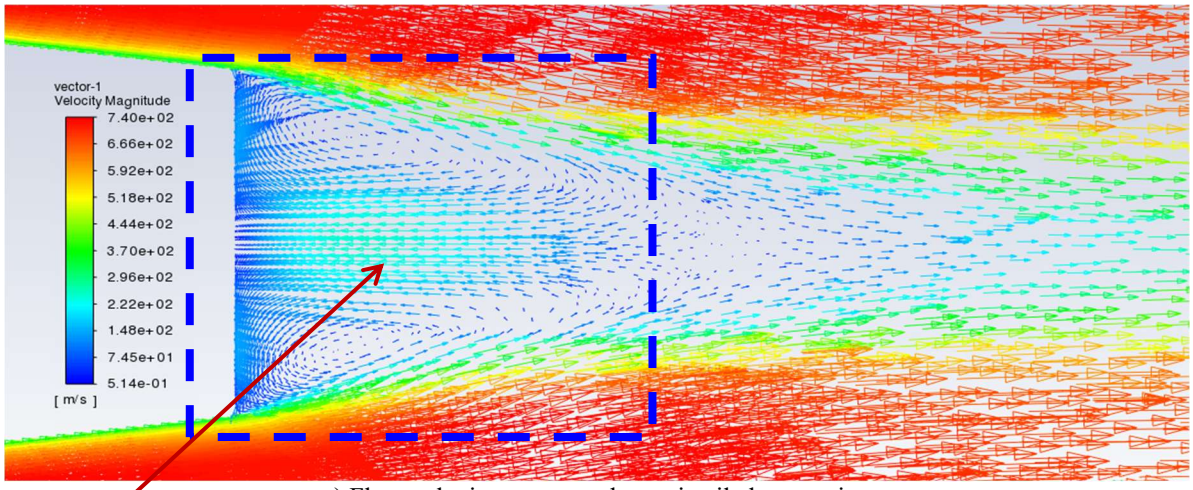

c) Flow velocity vector at the projectile base region

Figure 9 Visualization of the flow around BRL-1 projectile at Mach 2.0:
a) Density distribution around the projectile (top left)
b) Turbulence intensity distribution around the projectile (top right)
c) Flow velocity vector at the projectile base region (bottom)

The formation of oblique shock waves can be seen clearly in Figure 9.a, which is one of the characteristics of the supersonic flow. The pressure exerted on the projectile surface decreases from the projectile nose to the projectile base. The region with the largest turbulence intensity is the region directly behind the projectile base as seen in Figure 9.b. The flow velocity vector at the projectile base region is shown in Figure 9.c. The detachment of the flow from the projectile surface occurs at the end of the projectile boattail part which creates a recirculation flow region directly behind the projectile base. This backflow lowers the pressure acting on the projectile base which eventually leads to an increase in the base drag component.

IV. CONCLUSION

In this paper, the zero-lift drag coefficient of the small caliber spinning projectile BRL-1 was predicted at supersonic speeds using numerical simulation and semi-empirical methods. The total zero-lift drag coefficient was broken down into four different components, namely, pressure drag coefficient due to projectile nose, pressure drag coefficient due to projectile boattail, pressure drag coefficient due to projectile

base, and skin friction drag coefficient. The total zero-lift drag coefficient and its components obtained using numerical and semi-empirical methods were compared and analysed against available experimental data to evaluate the performance of each method. Based on the results obtained in this paper, several important conclusions can be drawn. Both numerical simulation and semi-empirical methods is capable of predicting zero-lift drag coefficient of a small caliber projectile with good accuracy for engineering applications. The overall trend of total drag as a function of Mach number is almost the same for two methods. However, quantitatively, the numerical prediction has shown less deviation from experimental data with an average deviation of 1.74%. From the Mach number of 2.2, the simulated total drag coefficient is nearly the same as the experimental data. Meanwhile, the semi-empirical method has predicted total zero-lift drag coefficient with an average deviation of 5.31%. The findings from the present study are significant contribution to better understanding of aerodynamics of small caliber supersonic spinning projectiles and have provided a practical guidance for appropriate selection of research methodology for aerodynamic prediction.

AUTHOR CONTRIBUTIONS

Q. T. Nguyen: Conceptualisation, methodology, literature review, simulation, formal analysis, data curation, result validation, writing - original draft, writing - review & editing.

REFERENCES

Braun, William F. (1973). Aerodynamic data for small arms projectiles. Report No. 1630, Ballistic Research Laboratories, Aberdeen Proving Ground, Maryland, USA.

De Briey, Vincent (2021). Small-Caliber Exterior Ballistics: Aerodynamic Coefficients Determination by CFD. Ph.D thesis, University of Liège, Belgium.

Ferfouri, A., **T. Allouche**, **D. Jerkovic**, **N. Hristov**, **M. Vuckovic**, & **A. Benmeddah (2023)**. Prediction of drag aerodynamic coefficient of the 155 mm projectile under axisymmetric flow using different approaches. *Journal of the Serbian Society for Computational Mechanics*, 17(2), 69–86.

Ko, A., **K. Chang**, **D. J. Sheen**, **C. H. Lee**, **Y. Park**, & **S. W. Park (2020)**. Prediction and analysis of the aerodynamic characteristics of a spinning projectile based on computational fluid dynamics. *International Journal of Aerospace Engineering*, 2020(1).

Mahdi, A. S., & **M. Al-Atabi (2008)**. Effect of body shape on the aerodynamics of projectiles at supersonic speeds. *Journal of Engineering Science and Technology*, 3(3), 278–292.

Matsson, J. E. (2023). An introduction to Ansys Fluent 2023. Mission, KS, USA: SDC Publications, ISBN: 978-1-63057-648-6.

McCoy, R. L. (1981). "Mc Drag" — A computer program for estimating the drag coefficients of projectiles. Technical Report ARBRL-TR-02293, Ballistic Research Laboratories, Aberdeen Proving Ground, Maryland, USA.

McCoy, R. L. (2009). *Modern Exterior Ballistics: The Launch and Flight Dynamics of Symmetric Projectiles* (2nd ed.). Schiffer Military History.

Menter, F. R. (1994). Two-equation eddy-viscosity turbulence models for engineering applications. *AIAA Journal*, 32(8), 1598–1605.

Moore, F. G., & **T. C. Hymer (2002)**. Improved semi-empirical method for power-on base-drag prediction. *Journal of Spacecraft and Rockets*, 39(1), 56–65.

Nguyen, Q. T., **H. M. Nguyen**, & **X. S. Bui (2024)**. Numerical investigation on the supersonic flow around a saboted bullet. *Vojnotehnički glasnik*, 72(2), 676–694.

Pokela, R. C., **D. Foster**, **M. Munroe**, **J. Koos**, **F. Mason**, **R. Kumar**, **B. McPherson**, & **R. H. Taylor (2021)**. Experimental study of axisymmetric projectile configurations at supersonic speeds. *AIAA Scitech 2021 Forum*.

Salunke, S., **S. Shinde**, **T. Gholap**, & **D. Sahoo (2023)**. Comparative computational analysis of NATO 5.56 mm, APM2 7.62 mm and AK-47 7.82 mm bullet moving at Mach 2.0 in close vicinity to the wall. *FME Transactions*, 51, 81–89.

Seretkaya, A. A., **C. Çalışkan**, & **S. Neşeli (2022)**. Comparison of real and simulation aerodynamic coefficients for 155 mm ammunition using open-source code SU2 software. *Politeknik Dergisi*, 25(4), 1835–1845.

Vasile, J. D., **J. Bryson**, & **F. Fresconi (2020)**. Aerodynamic design optimization of long range projectiles using Missile DATCOM. *AIAA Scitech 2020 Forum*.

Wanchai, J. (2014). Studies of aerodynamics of supersonic generic round shaped bodies. Ph.D thesis, Nanyang Technological University, Singapore.